JGR Atmospheres

RESEARCH ARTICLE
10.1029/2022JD038254

A Possible Cause for Preference of Super Bolt Lightning Over the Mediterranean Sea and the Altiplano

Avichay Efraim[1], Daniel Rosenfeld[1], Robert Holzworth[2], and Joel A. Thornton[3]

[1]Institute of Earth Sciences, The Hebrew University of Jerusalem, Jerusalem, Israel, [2]Department of Earth and Space Sciences, University of Washington, Seattle, WA, USA, [3]Department of Atmospheric Sciences, University of Washington, Seattle, WA, USA

Key Points:

- The lightning energy increases sharply as the distance between the charging zone and the surface decreases
- The lightning energy increases as the warm phase of the cloud decreases, and with a more developed cloud, but to a much lesser extent
- Aerosols play no significant role in determination of the lightning energy

Supporting Information:

Supporting Information may be found in the online version of this article.

Correspondence to:

A. Efraim,
avichay.efraim@mail.huji.ac.il

Citation:

Efraim, A., Rosenfeld, D., Holzworth, R., & Thornton, J. A. (2023). A possible cause for preference of super bolt lightning over the Mediterranean Sea and the Altiplano. *Journal of Geophysical Research: Atmospheres*, *128*, e2022JD038254. https://doi.org/10.1029/2022JD038254

Received 24 NOV 2022
Accepted 3 AUG 2023

Author Contributions:

Conceptualization: Avichay Efraim, Daniel Rosenfeld
Formal analysis: Avichay Efraim
Investigation: Avichay Efraim
Methodology: Avichay Efraim, Robert Holzworth
Resources: Robert Holzworth, Joel A. Thornton
Supervision: Daniel Rosenfeld
Visualization: Avichay Efraim
Writing – original draft: Avichay Efraim
Writing – review & editing: Avichay Efraim, Daniel Rosenfeld, Robert Holzworth

Abstract Exceptionally high-energy lightning strokes >10^6 J (X1000 stronger than average) in the very low-frequency band between 5 and 18 kHz, also known as superbolts (SB), occur mostly during winter over the North-East Atlantic, the Mediterranean Sea, and over the Altiplano in South America. Here we compare the World-Wide Lightning Location Network database with meteorological and aerosol data to examine the causes of lightning stroke high energies. Our results show that the energy per stroke increases sharply as the distance between the cloud's *charging zone* (where the cloud electrification occurs) and the surface decreases. Since the *charging zone* occurs above the 0°C isotherm, this distance is shorter when the 0°C isotherm is closer to the surface. This occurs either due to cold air mass over the ocean during winter or high surface altitude in the Altiplano during summer thunderstorms. Stroke energy decreases with the warm phase of the cloud, as proxied by the cloud base temperature, and increases with a more developed cloud, as proxied by the cloud top temperature, but to a much lesser extent than the distance between the surface and 0°C isotherm. Aerosols play no significant role. It is hypothesized that a shorter distance between the *charging zone* and the ground represents less electrical resistance that allows stronger discharge currents.

Plain Language Summary High-energy lightning bolts (super bolts), occur mostly during the winter in the North Atlantic, the Mediterranean Sea, and over North-West South America. In this study, we compare this energy, as obtained by a set of lightning detectors, with meteorological and aerosol data to test the causes that might determine the lightning energy level. The results of this study show that the lightning energy increases sharply when the distance between the *charging zone* (where the lightning generates) and the surface decreases. Since the *charging zone* occurs at altitudes above the level of 0°C, this distance is shorter when the level of 0°C is closer to the surface. This happens either due to cold air over the ocean during winter, or higher surface over the mountains in North-West South America during summer thunderstorms. The energy can also increase when the cloud precipitates more, but on a smaller scale than the distance between the surface and the *charging zone*. Aerosols play no significant role. It is speculated that a smaller vertical scale between the *charging zone* and the ground represents less electrical resistance, allowing higher currents and higher energies.

1. Introduction

The electrification in deep convective clouds occurs during the collision process of ice crystals and graupel particles in the mixed-phased zone. Upon collision, mostly negative electrical charges are transferred from the ice crystals to the graupel. The positively charged ice crystals ascend with the updrafts, whereas the negatively charged heavier graupel fall gravitationally, thus building an electric field that leads to an electrostatic discharge, known as a lightning stroke (Dwyer & Uman, 2014; Kang et al., 2023; Reynolds et al., 1957; Takahashi, 1978; Williams, 1988). Lightning discharges are very powerful impulsive sources of electromagnetic energy that range over a wide bandwidth (Magono, 1980), where the bulk of the radiated energy is in the very low frequency (VLF) bands <30 kHz (Pierce, 1977). The World-Wide Lightning Location Network (WWLLN) is a set of radio wave detectors that exploits the radiated energy and detects the time, location, and energy of each lightning stroke (Hutchins, Holzworth, Rodger, & Brundell, 2012; Lay et al., 2004; Rodger et al., 2004, 2006). Since the VLF electromagnetic energy propagates with low attenuation between the conducting Earth and the lower boundary of the ionosphere (Rodger et al., 2006), the signals can be received within thousands of kilometers from the source (Crombie, 1964), allowing the WWLLN a global coverage of lightning detection. It is important to note that the WWLLN energy is directly related to the peak current ±25% for typical stokes (Hutchins, Holzworth, Rodger, & Brundell, 2012). Therefore, knowing the WWLLN energy is tantamount to knowing the peak current. So, one

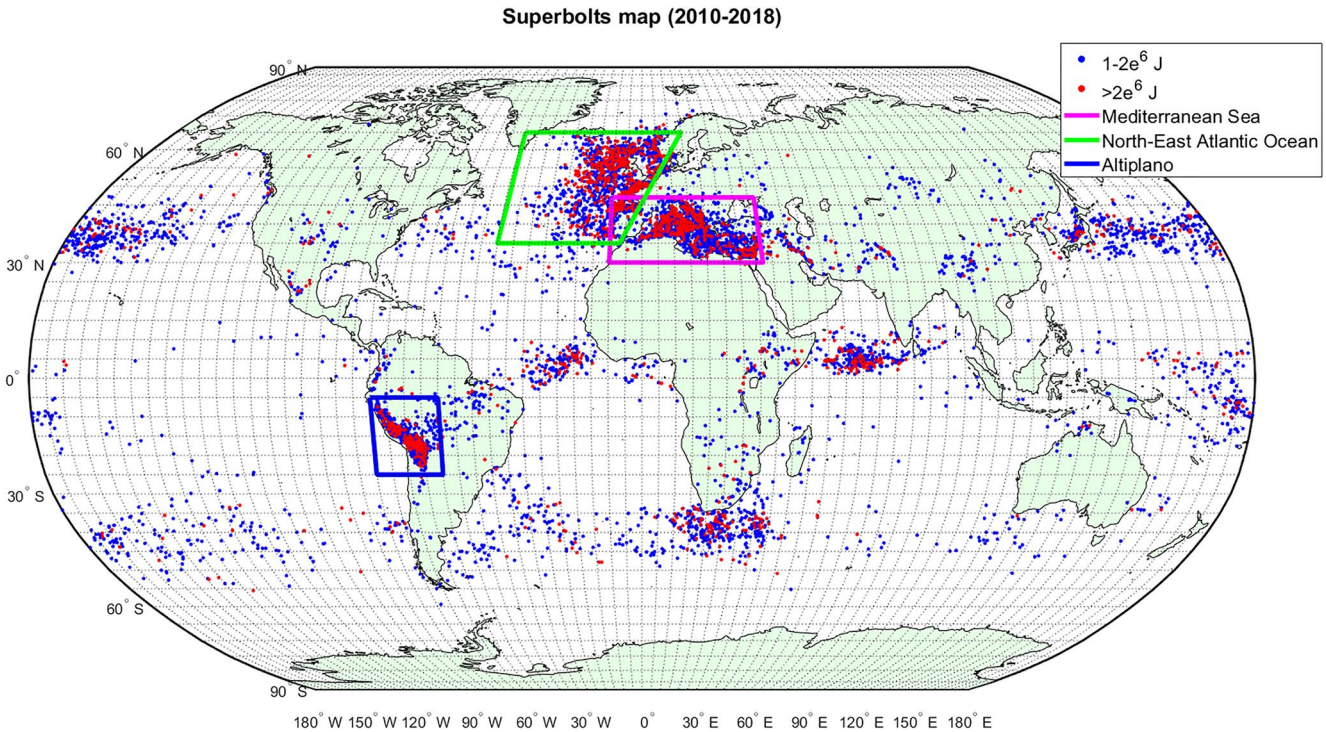

Figure 1. Global distribution of all superbolts between 2010 and 2018. The blue points are lightning strokes with 1–2e^6 J, and the red points are with >2e^6 J. Adapted from Holzworth et al., 2019. The polygons are the regions with the most detected and strongest SB: (1) The Mediterranean Sea (magenta); (2) the North-East Atlantic Ocean (green); and (3) the Altiplano (blue).

can reasonably use either peak current data or WWLLN stroke energy data to be equivalent markers for lightning strength. In this paper, we used the WWLLN as it was more available and accessible.

Superbolts (SB) are exceptionally high-energy lightning strokes, with detected energy of above 10^6 J, which is three orders of magnitude higher than the mean energy per stroke of 10^3 J (Holzworth et al., 2019; Turman, 1977). Holzworth et al. (2019) used WWLLN to map the SB for 2010–2018 (Figure 1). According to the map, the SB occur globally and mostly over extra-tropical water. That is contrary to the global distribution of all lightning which shows about 10 times more strokes mainly over tropical continents than over oceans (Christian et al., 2003; Lay et al., 2007). Although SB can occur anywhere in the world, there are three main regions with the most detected and strongest SB (Figure 1): (a) the North-East Atlantic Ocean (NEAO) from ∼20°W to the European coastlines, and from the latitude of Spain to mid-Norway; (b) The Mediterranean Sea (MS); and (c) the Altiplano in South America. The majority of the SB (∼76%) occur during the northern hemisphere winter (November until February) (Holzworth et al., 2019), and constitute only ∼0.00045% of the total lightning strokes (Kirkland, 1999; Turman, 1977; Yair et al., 2021). The causes for the spatial and temporal distribution of SB remain unknown.

Nonetheless, there have been some speculations as to what might determine the energy per stroke. One theory, suggested by Asfur et al. (2020), says that lightning above saltier water are more intense. Asfur et al. (2020) described a lab experiment of discharges into saline water. The intensity of the discharges increased exponentially with the salinity of the water. Thus, they hypothesized that the higher conductivity of saline water, compared to moist soil, results in a more efficient discharge to the surface, a larger peak current, a brighter optical flash, and higher energy per stroke. However, it does not explain the similar frequency of SB over the Mediterranean and North Seas despite the differences in their salinity (Figure S1 in Supporting Information S1), nor can it explain the SB over the Altiplano. The soil salinity over rainy equatorial regions that includes the Altiplano is much smaller than the oceans (Ivushkin et al., 2019). Another theory was suggested by Yair et al. (2021) who presented the climatology of the east-Mediterranean SB. They suggest that such SB are more abundant in the presence of large amounts of desert dust aerosols, coming from the Sahara Desert. The dust is ingested into the marine clouds and contributes to convective invigoration, enhanced freezing, and efficient charge separation. However, much like the Asfur et al. (2020) theory, the Yair et al. (2021) theory cannot explain the similarly intense SB over the NEAO.

A third theory was suggested by Pizzuti et al. (2022) who examined the SB over Northern and Western Europe during 2010–2020. They claim that the advection of sea spray aerosols and busy shipping lane emissions contribute to the convective invigoration that leads to enhanced cloud electrification over the English Channel compared to surrounding areas. Like the previously suggested theories, this one also discusses only a specific region and cannot explain the dearth of SB in other rainy regions with similar shipping density. In addition, the effects of fine ship emission aerosols and coarse sea spray (CSS) aerosols on invigoration are of opposite signs (Pan et al., 2022).

Eventually, the three above-mentioned studies (Asfur et al., 2020; Pizzuti et al., 2022; Yair et al., 2021) focus on specific regions and only above bodies of water (the MS and NEAO). Therefore, they might explain at best only part of the spatial distribution of the SB, but not all three main regions of SB occurrence, especially not the conspicuous SB region of the Altiplano.

As for the SB temporal distribution, Brook et al. (1982) showed that during winter thunderstorms the positive polarity lightning peak currents are stronger. They related it to the wind shear, as a more intense wind shear in winter thunderstorms results in a lateral separation between the charges. This separation ensures the initiating positive streamer toward the ground, instead of toward the negatively charged region that typically lies right beneath it. On the other hand, Orville et al. (1987) showed that the peak currents of lightning with both polarities were higher in the winter than in the summer. In addition, Brook (1992) showed that radiation associated with electric field breakdown is greater in winter than in summer in thunderstorms over Albany, New York. A higher electric field results in a higher accumulation of charge before the breakdown, where the electrostatic energy density goes up as the square of the electric field (Griffiths, 2018). The higher electric field can be found in clouds with smaller drops, because the presence of large drops (free water surface), lowers the breakdown voltage (Brook, 1992). According to Brook (1992), such was the case in the examined winter storms over Albany—saturation vapor pressure close to that over ice, which leads to the formation of ice at the expense of liquid water (Wegener–Bergeron–Findeisen process) and eventually little deformable liquid water for discharge initiation.

In addition, high precipitation rates in clouds with large drops increase the electrical conductivity (Kamra, 1979), which leads to earlier and weaker breakdown voltage. Another suggested factor that might affect the breakdown is the air density, where denser air leads to higher dielectric strength and a higher needed breakdown voltage, thus stronger lightning (Hirsh & Oskam, 1978).

Here we suggest a new hypothesis for the occurrence of SB, based on the robust results presented in this study. The hypothesis, which is suitable for both over land and ocean, as opposed to the theories of Asfur et al. (2020), Yair et al. (2021), and Pizzuti et al. (2022); and relates to the observations of both Orville et al. (1987), Brook (1992) and Holzworth et al. (2019), states that the main factor that sets the energy per stroke is the vertical distance between the *charging zone* and the surface, where shorter distance results in higher energy. The *charging zone* is the ice and supercooled water mixed phase zone of the cloud, in which the charge separation occurs (Williams et al., 1991). The altitude of charge separation within the *charging zone* depends on the updraft, collision rate, temperature, and cloud water content (Li et al., 2020; Pereyra et al., 2008; Reynolds et al., 1957; Takahashi, 1978). Thus, the strict lowest boundary of this zone is marked by the height of the 0°C isotherm. Unfortunately, WWLLN does not distinguish the polarity of each stroke, so this aspect could not be addressed in this study.

Further description and discussion of the new theory are presented in Section 3, preceded by the methodology in Section 2.

2. Methodology

In this study, the energy per lightning stroke was examined as a function of different variables of the thunderstorm in various regions of interest (ROI).

The time, location, and energy of each lightning stroke were obtained from the WWLLN database (WWLLN, 2022, http://wwlln.net). WWLLN is active since August 2004 and detects lightning anywhere in the world with an accuracy of ∼5 km and in a high-temporal resolution (Abarca et al., 2010; Holzworth et al., 2019; Hutchins, Holzworth, Brundell, & Rodger, 2012; Jacobson et al., 2006; Rodger et al., 2006). It consists of a set of over 80 globally spread VLF radio receivers (100 Hz–24 kHz) (Holzworth et al., 2019). These receivers identify the time of group arrival (TOGA) for the wave packets of individual lightning sferics (Dowden et al., 2002). The TOGA times, with an accuracy of ∼1 μs, from five or more WWLLN stations, are then used to determine the source

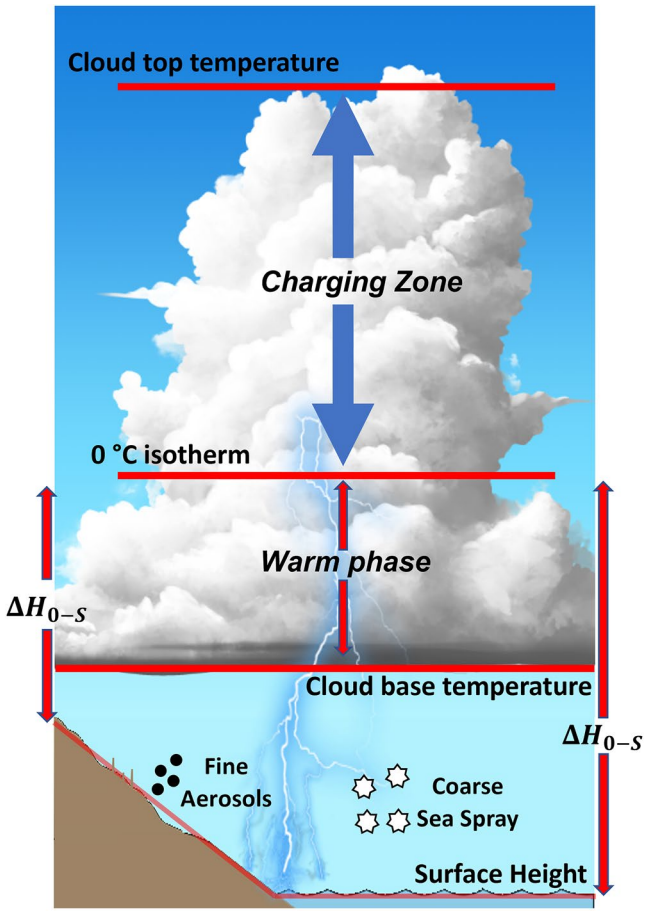

Figure 2. Illustration of deep convective cloud, with the thunderstorm and environmental properties as described in Section 2.

location of the lightning stroke by triangulation (Dowden & Brundell, 2000; Hutchins, Holzworth, Brundell, & Rodger, 2012; Rodger et al., 2006, 2009).

Lightning discharge of electromagnetic waves occurs over a wide spectrum. The long-wave radio frequencies propagate with low attenuation between the conducting Earth and the lower boundary of the ionosphere (Rodger et al., 2006) thus enabling the detection of VLF signals thousands of kilometers from the source. The calculation of the energy per stroke for each WWLLN detected lightning is done by using the root mean square (RMS) of the electric field during each sferic interval (Hutchins, Holzworth, Rodger, & Brundell, 2012). This value is obtained in the 6–18 kHz band over the triggering window of 1.33 ms. Then, the U.S. Navy Long Wave Propagation Capability algorithm (Ferguson, 1998; Thomson, 2010) models the VLF propagation from each detected stroke and determines the necessary energy to produce the measured RMS electric field (in the VLF band) at each WWLLN station (Hutchins, Holzworth, Rodger, & Brundell, 2012). The WWLLN has a relatively high daily and global detection efficiency (Holzworth et al., 2019; Hutchins, Holzworth, Brundell, & Rodger, 2012). However, to ensure the data are not biased or contaminated, only lightning with standard error in the fit for energy of less than 30%, and that were detected by at least seven WWLLN stations were considered (Holzworth et al., 2019). Each stroke's time and location were used to extract certain properties of the thunderstorm and the environment. The energy per stroke from WWLLN was then analyzed as a function of these properties. The said variables and their source are described as follows and illustrated in Figure 2:

1. *Surface Height* (H_{SFC})—the altitude at the closest pixel below the detected stroke coordinates. These data were obtained from the GEBCO (General Bathymetric Chart of the Oceans) database. The GEBCO is a high-resolution raster of heights that maps both the ocean's bathymetry and the land surface height. Its spatial resolution is 15 arc-seconds which corresponds to ~450 m at the equator and less in higher latitudes. In this study, only the land surface height data were considered, and the oceans' surface height was set to 0 m.
2. 0°C *isotherm height* (H_0)—the bottom height of the *charging zone*. Since the electrical charge separation occurs at subfreezing temperatures somewhere in the *charging zone*, the bottom boundary of this microphysical zone was taken. This is under the assumption that temperature decreases with height during atmospheric unstable conditions that are conducive to thunderstorms. The data were acquired from the National Centers for Environmental Prediction (NCEP) Final Operational Global Analysis data. The spatial resolution of NCEP is 2.5° latitude × 2.5° longitude and its temporal resolution is 4 × daily (every 6 hr) (Kanamitsu et al., 2002).
3. *Cloud base temperature* (*CBT*)—this variable was calculated by the 2-m temperature and the lifting condensation level, using the dry adiabatic lapse rate. These data were obtained from the Modern-Era Retrospective Analysis for Research and Application Version 2 (MERRA-2) reanalysis data. The MERRA-2 is a NASA meteorological reanalysis data set that uses the Goddard Earth Observing System Data Assimilation System version 5. This data set contains atmospheric components, meteorology characteristics as well as aerosols and atmospheric chemical constituents at a spatial resolution of 0.5° latitude × 0.625° longitude × 72 pressure levels and a temporal resolution of 24 X daily (every 1 hr) for the meteorological data and 8 × daily (every 3 hr) for the aerosol data (Gelaro et al., 2017). The CBT is used to determine the thickness of the warm phase at a constant H_0 to H_{SFC} difference, which controls the potential of precipitation and the presence of graupel in the *charging zone*.
4. *Cloud top temperature* (*CTT*)—the *charging zone* upper boundary. The CTT can be used as a proxy for the vertical development of the cloud, or the thickness of the *charging zone*, where colder CTT means a more developed cloud. The CTT data were also obtained from the MERRA-2 reanalysis data.

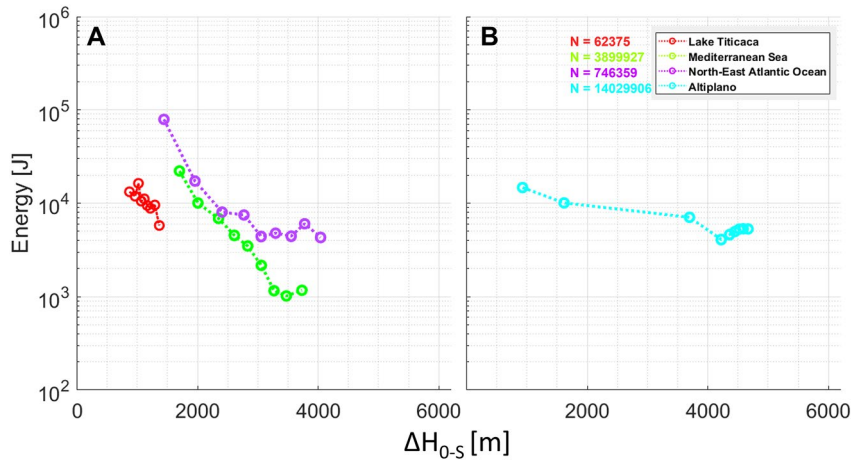

Figure 3. The mean energy per stroke as a function of the distance between the 0°C isotherm height and the surface height ($\Delta H_{0\text{-}S}$) for Lake Titicaca (red), the Mediterranean Sea (green), and the North-East Atlantic Ocean (purple) in panel (a), and for the Altiplano (cyan) in panel (b). The lightning cases are binned in intervals of 10 percentiles in all regions. The total number of data points for each region is shown on the plot.

5. *FA*—Boundary layer fine aerosol concentration (dry radius < 1 μm (Pan et al., 2022)). These data are from the MERRA-2 data set as well. MERRA-2 aerosol data have five aerosol classes: dust, sea salt, sulfates, organic carbon, and black carbon (Buchard et al., 2015). According to the aerosol radius bin classification on the MERRA-2 website, the following aerosol types were considered as FA: hydrophilic and hydrophobic black carbon, hydrophilic and hydrophobic organic carbon, sulfate aerosols, and fine sea salt.
6. *CSS*—Boundary layer CSS aerosol concertation (dry radius > 1 μm (Pan et al., 2022)). These data were also obtained from MERRA-2 and include the coarse sea salt aerosol concentration.

The lightning analyses in this study were done in three ROI (Figure 1): (a) the MS, (b) the Altiplano in South America (AP), and (c) the NEAO. We note here that the SB global distribution map (Figure 1) also has a relatively larger density of the strongest SB (over 2×10^6 J (red dots)) along the equator in the Atlantic and Indian Oceans, south of South Africa, and between ~40°N and 40°S in the Pacific Ocean. However, to test our hypothesis, we focused on cases either where the H_0 is lower, that is, during the northern hemisphere winter or the H_{SFC} is higher. According to Holzworth et al. (2019), the vast majority of the strongest SB occur during the northern hemisphere winter in these ROI and not elsewhere in the extratropics. Along the tropical oceans, H_0 remains fairly constant during the year; therefore, the hypothesis is not relevant to such cases.

Although SB constitute a small percentage of the total detected strokes per year, this study examines the conditions that may cause the highest energy of all the detected strokes and not just the defined SB. The analysis was done for data during 2013–2015, which are characterized by a high occurrence of SB (Holzworth et al., 2019). The total numbers of detected strokes over the different ROI are ~3.9×10^6 over the MS, ~7.46×10^5 over the NEAO, and ~14×10^6 strokes over the AP. Detailed maps of the ROI are shown in Figure S2 in Supporting Information S1.

3. Results and Discussion

Our main hypothesis is that lightning strokes are more energetic when the vertical distance between the *charging zone* and the surface is shorter. To test this hypothesis, Figure 3 presents the mean stroke energy in 10 percentile intervals (J) as a function of the vertical distance between H_0 and H_{SFC} ($\Delta H_{0\text{-}S}$ [m]) for the MS and NEAO (Figure 3a), and for the AP (Figure 3b). Within the AP lies Lake Titicaca which is a large body of water. Therefore, it was added to the analysis with the other bodies of water in Figure 3a.

Over the MS and NEAO, H_{SFC} is 0 m and the H_0 ranges between ~700 and ~4,000 m (Figure 3a). It is clearly shown that for these regions the energy decreases sharply as $\Delta H_{0\text{-}S}$ increases. Over the NEAO the lightning reaches higher energy and in both regions, there is a stabilization when the distance exceeds ~3,000 m.

The H_0 over the whole AP (Figure 3b) has a much lower variability compared to the other two regions (mean: ~4,700 ± 200 m year-round) because the rainfall there occurs from tropical convection which always has a nearly

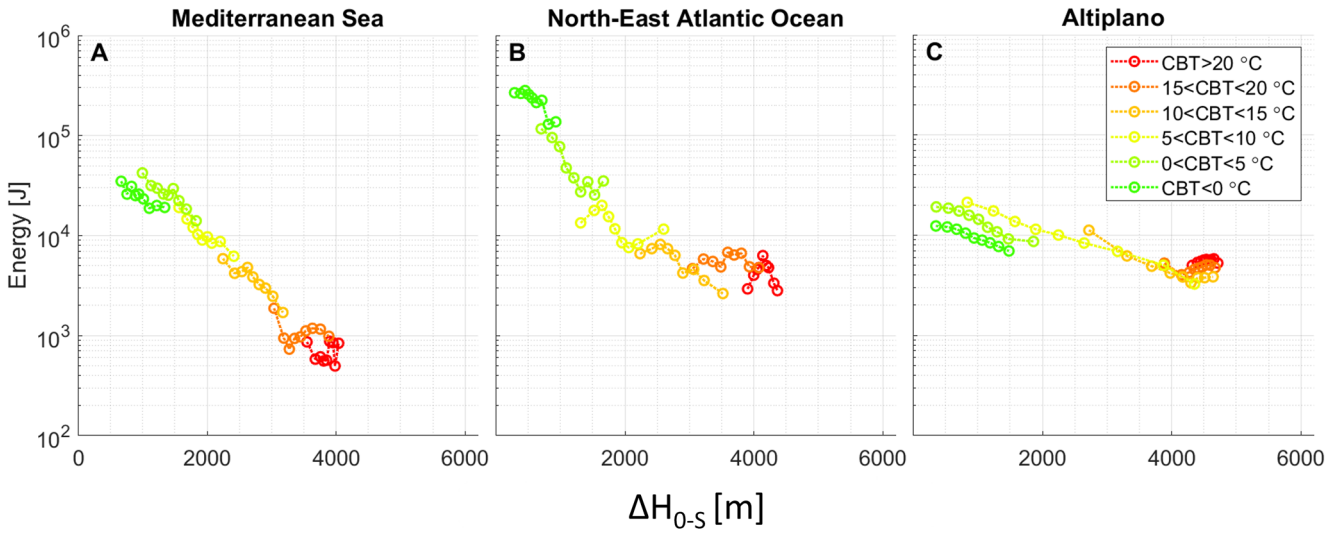

Figure 4. The mean energy per stroke as a function of the $\Delta H_{0\text{-}S}$ for (a) the Mediterranean Sea, (b) North-East Atlantic Ocean, and (c) the Altiplano. The color of the lines indicates the cloud base temperature bins. The data are binned by the same percentiles as in Figure 3 and the total number of data points for each region is the same as shown in Figure 3.

constant H_0 (Garreaud et al., 2003; Harris et al., 2000; Schauwecker et al., 2017). However, the H_{SFC} ranges between sea level and ~5,000 m. Overall, the $\Delta H_{0\text{-}S}$ trend is similar to the trend over the bodies of water but the variability in the energy is much lower. Two possible explanations for that are (a) the peak points over land with very high local voltage gradient that might trigger lightning with lower breakdown voltage compared to the flat surface of the oceans; (b) and the lower air density in these altitudes that might lead to lower dielectric strength and weaker strokes. This might also explain the case of Lake Titicaca. It behaves similarly to the slope of the plots of the other bodies of water but with lower energy lightning like the AP that surrounds it.

Based on these results, it seems that for both land and ocean, our hypothesis is supported and the factor that determines the energy per stroke is the vertical distance between the surface and the *charging zone*. However, other factors were examined as well.

The first one is the thickness of the warm phase of the cloud, which can be used as a proxy for the warm precipitation depth and rate. As mentioned above, clouds with fewer large drops and lower precipitation rates, have higher breakdown voltage and stronger strokes. So, a thicker warm phase means a higher rain rate. Therefore, the breakdown voltage and the lightning energy are expected to be lower. The warm phase thickness is reflected in the change of CBT for a constant $\Delta H_{0\text{-}S}$, where a warmer CBT means a thicker warm phase. Figure 4 shows the mean stroke energy (J) as a function of $\Delta H_{0\text{-}S}$ (m) binned by CBT intervals.

The red line is the warmest CBT (>20°C), and the green line is the coldest one (<0°C) which corresponds to higher and lower $\Delta H_{0\text{-}S}$, respectively (Figure S3 in Supporting Information S1).

Since both lower $\Delta H_{0\text{-}S}$ and colder CBT correlate with higher energy values, the CBT does not add significant information to the overall trend. Although, there are some overlapping cases with the same low $\Delta H_{0\text{-}S}$ over the MS and AP, where the warmer CBT result in slightly higher energy. These small deviations might indicate other possible CBT-related factors.

Another factor that might affect the energy is the level of cloud development or the thickness of the *charging zone*. Several observational studies have shown that for the same cloud base height, higher cloud tops promote cloud electrification and increase the lightning rate due to enhanced charge separation (Atchley, 1983; Lhermitte & Williams, 1984; Williams, 1985, 2001; Williams et al., 2005).

Figure S4 in Supporting Information S1 presents the energy per stroke as a function of the flash rate for the different ROI. The lightning strokes were related to the same storm by taking strokes within 5 km of each other and within a time frame of 20 min. Then, adjacent lightning (spatially and temporally) were examined, and the time between them was calculated. This results in the lightning frequency (or flash rate) in units of s^{-1}. Figure

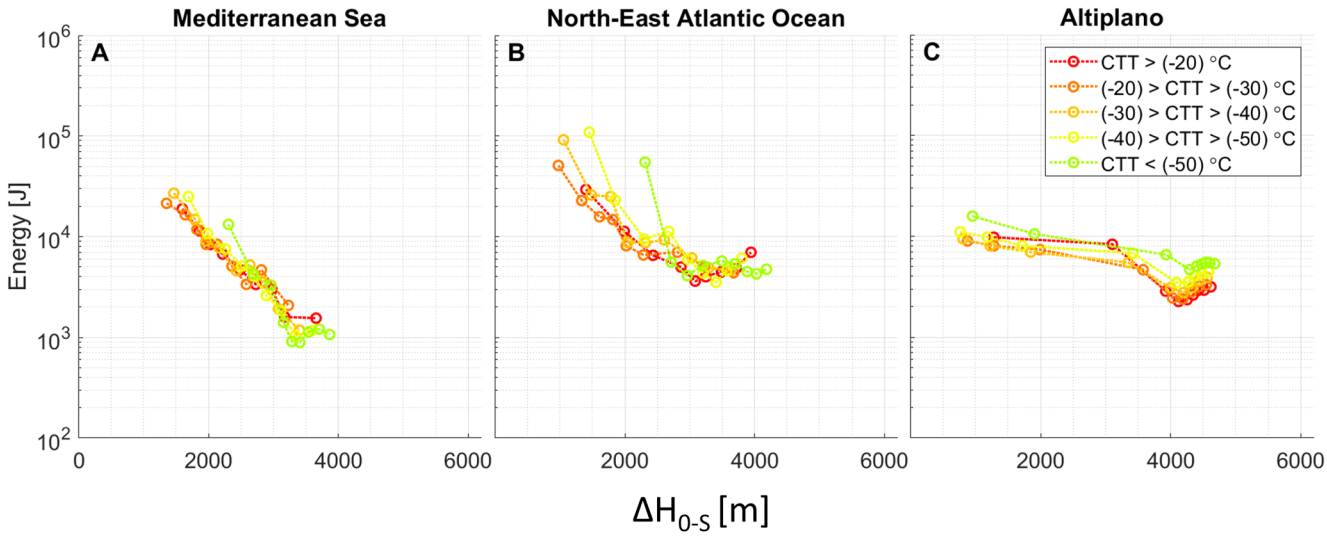

Figure 5. The mean energy per stroke as a function of the $\Delta H_{0\text{-}S}$ for (a) the Mediterranean Sea, (b) North-East Atlantic Ocean, and (c) the Altiplano. The color of the lines indicates the cloud top temperature bin. The data are binned by the same percentiles as in Figure 3 and the total number of data points for each region is the same as shown in Figure 3.

S4 in Supporting Information S1 as well as the work of Chronis et al. (2015) and Chronis and Koshak (2017), present evidence for higher energy at low flash rates, which is typical to the winter and cool-base storms. The thickness of the *charging zone* can be inferred from the CTT, where a more developed cloud reaches higher altitudes and colder temperatures for the same H_0. Figure 5 shows the energy as a function of the $\Delta H_{0\text{-}S}$ binned by the CTT. Considering the effect of the flash rate, we would expect that colder CTT (toward the green line) would result in lower energy. However, Figure 5 shows a different behavior than the expected one: for the same $\Delta H_{0\text{-}S}$ values, colder CTT (more developed cloud), results in slightly higher energy. Over the MS and NEAO it is most noticeable in the lower $\Delta H_{0\text{-}S}$ values (Figures 5a and 5b), and over the AP (Figure 5c) it seems to be more significant over the higher $\Delta H_{0\text{-}S}$ values. This could be explained by Han et al. (2021) who recently showed the non-linearity of the flash rate as a function of the ice fraction, where more developed clouds are expected to have more ice. When the ice fraction is rather small, the clouds are governed by liquid droplets with no efficient charge separation, thus lower flash rate and higher energy. As the ice fraction increases to an optimum point, the clouds tend to have sufficient ice hydrometeors and supercooled droplets to produce the most lightning activities efficiently. Beyond that optimum point, the ice phase becomes dominant, and the cloud experience less efficient charge separation again, which lowers the lightning rate and increases the energy. In any case, the thickness of the charging zone impacts the energy per stoke on a much smaller scale than the $\Delta H_{0\text{-}S}$.

A third speculated factor is the aerosols effect. Pan et al. (2022) showed that adding fine aerosols (FA) increases the lightning density significantly while adding coarse sea spray (CSS) weakens it. Figure 5 shows the mean stroke energy (J) as a function of $\Delta H_{0\text{-}S}$ (m) binned by boundary layer FA (Figures 5a–5c) and CSS (Figures 5d and 5e) concentration intervals. The CSS concentration over the AP is not shown since it is negligible over land. As shown in the figure, the contribution of the different classes of aerosols does not have a significant effect on the detected energy as it does on the lightning density.

Our results (Figures 3–6) support the following possible physical explanation: when the vertical distance between the *charging zone* and the surface is shorter, the *charging zone* is less isolated from the ground. The column of isolating air is shorter and there is less electrical resistance in the lightning channel. Therefore, the electrical current is enhanced, and the indicated energy is larger. This hypothesis might hint at the mechanism of a capacitor. The electric field strength in a capacitor is directly proportional to the voltage applied and inversely proportional to the distance between the plates, that is, $E = \frac{V}{d}$. By reducing the length of the discharge channel (d), the resistive-capacitive (RC) time constant of discharge is also shortened, resulting in an increase in peak current for the same amount of charge transfer. On the other hand, a shorter channel length (or antenna) may lead to a decrease in the radiated energy for the same channel current. This discrepancy can be solved by the fact that lightning have not only vertical channels but also horizontal ones (Mazur et al., 1998). Therefore, smaller $\Delta H_{0\text{-}S}$ do not necessarily decrease the radiated energy.

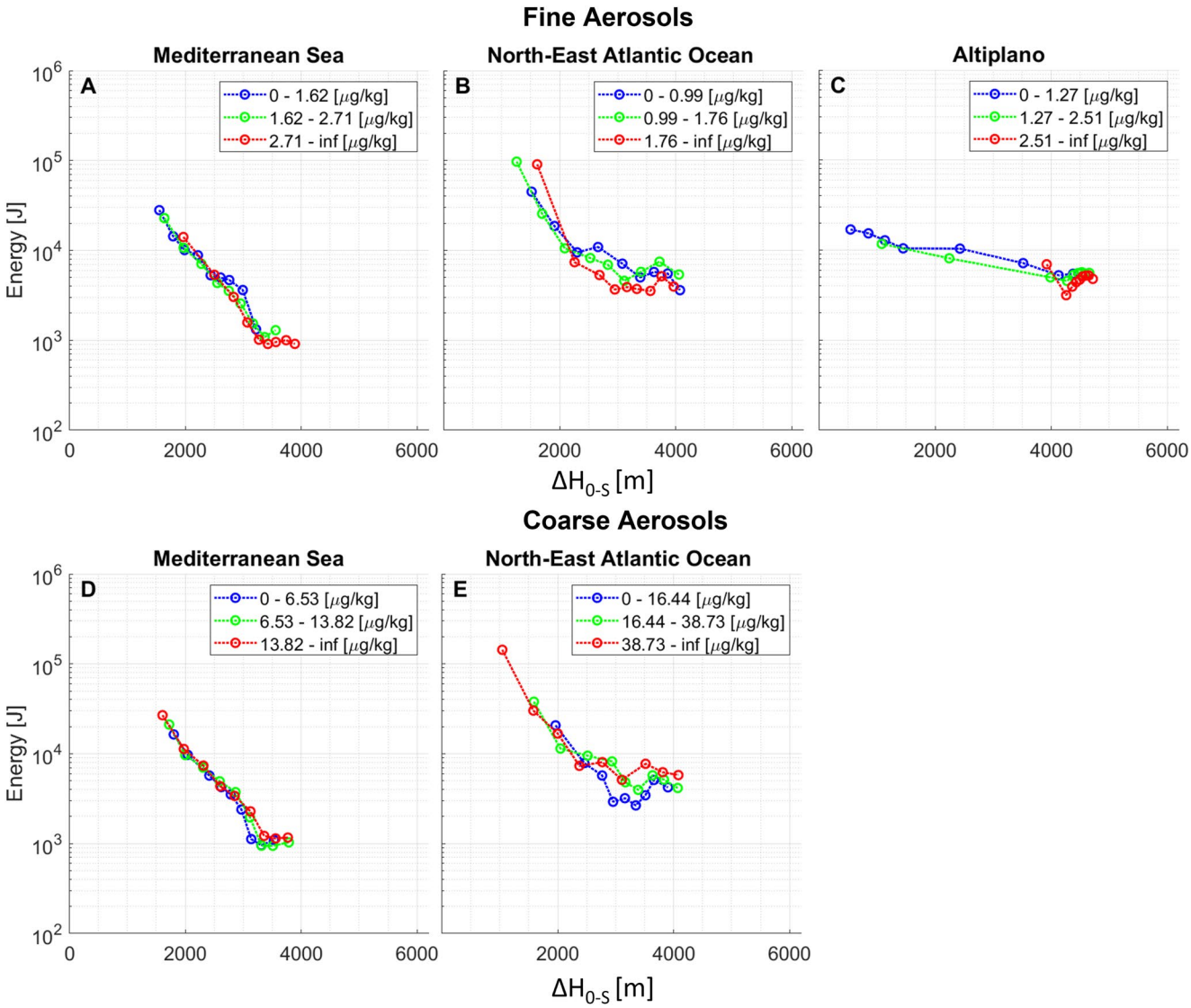

Figure 6. The mean energy per stroke as a function of the $\Delta H_{0\text{-}S}$ for (a, d) the Mediterranean Sea, (b, e) North-East Atlantic Ocean, and (c) the Altiplano. The color of the lines indicates the boundary layer fine aerosol (a–c) and coarse sea spray (CSS) (d, e) concentration intervals. The particle mixing ratio intervals in each panel are determined by the percentiles: 0%–30%, 30%–60%, and 60%–100%. The CSS concentration is negligible over land and thus is not shown over the Altiplano. The data are binned by the same percentiles as in Figure 3 and the total number of data points for each region is the same as shown in Figure 3.

The lowered *charging zone* can also imply a larger breakdown voltage (V), due to the higher density of the surrounding air. In addition, colder CBT which means a thinner warm phase lowers the rain rate and causes an increase in the breakdown voltage.

Overall, the increase of V and decrease of d increase the electric field (E), which allows for more accumulation of charge before the breakdown, and higher lightning energy.

In contrast to the previous theories presented above (Asfur et al., 2020; Pizzuti et al., 2022; Yair et al., 2021), which explain only part of the global distribution of SB and only above bodies of water, this theory applies both over land and ocean.

Alongside our proposed physical explanation, we acknowledge the possibility that there may be other factors and phenomena that contribute to the global SB distribution. One such factor is the magnitude of charge (Q) present in the charging zone. It is possible that a combination of a large Q with a large $\Delta H_{0\text{-}S}$ or a smaller Q with a shorter $\Delta H_{0\text{-}S}$ could produce the same effect on the lightning energy. However, since we do not have data on Q, we can

only speculate on this connection without definitive proof. In addition, as discussed above regarding Figure 5, the discrepancy between the expected and the observed behavior could be explained by the non-linearity of the ice fraction to flash rate ratio. However this a speculation that might require validation, since the development level of the cloud is merely a proxy for the ice content.

We emphasize that this paper suggests a possible physical explanation based on the robust observations in the three main regions with the most SB over the globe. Analyses of different ROI, other than the three mentioned here, and with a broader set of data to test and suggest other possible explanations and phenomena for the SB were left for future studies.

4. Summary

This study presents a new theory that might explain what causes exceptionally energetic lightning strokes also known as superbolts (SB). The SB are globally spread with three main hotspots of high concentration in the NEAO, the MS, and the Altiplano in South America. The electrification in deep convective clouds occurs within the mixed phase microphysical zone of supercooled droplets, ice crystals, and graupel particles. This microphysical zone is referred to as the *charging zone* where the level of the 0°C isotherm is its lower boundary. Analyzing the energy per stroke as a function of the distance between the *charging zone* and the surface, the cloud base and top temperature, and the boundary layer fine and coarse aerosol concentrations resulted in clear insights. The most conspicuous result shows that the energy per stroke decreases sharply as the distance between the *charging zone* and the surface increases. We hypothesize that when the distance between the *charging zone* and the surface is shorter, the *charging zone* is less isolated from the ground and there is less electrical resistance, which leads to more electrical current and larger indicated energy. Colder cloud base temperature, which is a proxy for a thinner warm phase, also correlates with high energy values, due to a lower rain rate. The lower rain rate decreases the air conductivity and allows for higher breakdown voltage. It was also found that a cloud with a colder top temperature, which is a proxy for the vertical development of the cloud, results in slightly higher energy for the same *charging zone* to surface distance. This opposes the considerations of a higher flash rate in developed clouds that should reduce the energy but agrees with the higher ice faction consideration expected in more developed clouds. The added FA or CSS do not seem to have a significant impact on the detected energy.

These findings and possible physical explanations are valid for lightning over both land and ocean, as opposed to previously suggested theories that explained only part of the picture and are based on our robust results. However, further research is required to cover other regions and to further substantiate the hypothesis and additional explanations.

Conflict of Interest

The authors declare no conflicts of interest relevant to this study.

Data Availability Statement

The WWLLN data used in this study are available at a nominal cost from http://wwlln.net/ WWLLN (2022). The GEBCO data are available on the GEBCO website (GEBCO Compilation Group, 2022). The NCEP reanalysis data are available on the NCEP website (National Centers for Environmental Prediction et al., 2000) after free registration. The MERRA-2 reanalysis data are available on the Global Modeling and Assimilation Office (GMAO) website (GMAO, 2015).

Acknowledgments
The authors wish to thank the WWLLN project (http://wwlln.net), a collaboration among over 50 universities and institutions, for providing the lightning data used in this paper. The authors would also like to express their sincere gratitude to Earl Williams for his valuable critique, which greatly contributed to the improvement of this paper. Special thanks goes also to Lior Efraim for clearing time for work and for her moral support. This study is supported by the BSF Grant 2020809 and the NSF Grant AGS-2113494.

References

Abarca, S. F., Corbosiero, K. L., & Galarneau, T. J. (2010). An evaluation of the worldwide lightning location network (WWLLN) using the national lightning detection network (NLDN) as ground truth. *Journal of Geophysical Research*, *115*(D18), D18206. https://doi.org/10.1029/2009JD013411

Asfur, M., Price, C., Silverman, J., & Wishkerman, A. (2020). Why is lightning more intense over the oceans? *Journal of Atmospheric and Solar-Terrestrial Physics*, *202*, 105259. https://doi.org/10.1016/j.jastp.2020.105259

Atchley, A. (1983). TRIP 1979: Case study of August 7 thunderstorm over Langmuir Laboratory. In L. H. Ruhnke, J. Latham, & A. Deepak (Eds.), *Proceedings in atmosphere electricity*.

Brook, M. (1992). Breakdown electric fields in winter storms. *Journal of Atmospheric Electricity*, *12*(1), 47–52. https://doi.org/10.1541/jae.12.47

Brook, M., Nakano, M., Krehbiel, P., & Takeuti, T. (1982). The electrical structure of the Hokuriku winter thunderstorms. *Journal of Geophysical Research*, *87*(C2), 1207–1215. https://doi.org/10.1029/JC087iC02p01207

Buchard, V., da Silva, A. M., Colarco, P. R., Darmenov, A., Randles, C. A., Govindaraju, R., et al. (2015). Using the OMI aerosol index and absorption aerosol optical depth to evaluate the NASA MERRA aerosol reanalysis. *Atmospheric Chemistry and Physics*, *15*(10), 5743–5760. https://doi.org/10.5194/acp-15-5743-2015

Christian, H. J., Blakeslee, R. J., Boccippio, D. J., Boeck, W. L., Buechler, D. E., Driscoll, K. T., et al. (2003). Global frequency and distribution of lightning as observed from space by the Optical Transient Detector. *Journal of Geophysical Research*, *108*(D1), ACL4-1–ACL4-15. https://doi.org/10.1029/2002JD002347

Chronis, T., Cummins, K., Said, R., Koshak, W., McCaul, E., Williams, E. R., et al. (2015). Climatological diurnal variation of negative CG lightning peak current over the continental United States. *Journal of Geophysical Research: Atmospheres*, *120*(2), 582–589. https://doi.org/10.1002/2014JD022547

Chronis, T., & Koshak, W. J. (2017). Diurnal variation of TRMM/LIS lightning flash radiances. *Bulletin of the American Meteorological Society*, *98*(7), 1453–1470. https://doi.org/10.1175/BAMS-D-16-0041.1

Crombie, D. D. (1964). Periodic fading of VLF signals received over long paths during sunrise and sunset. *Journal of Research of the National Bureau of Standards, Section D: Radio Science*, *27*.

Dowden, R. L., & Brundell, J. B. (2000). Improvements relating to the location of lightning discharges. *Australia Patent*, *749713*, 200071483.

Dowden, R. L., Brundell, J. B., & Rodger, C. J. (2002). VLF lightning location by time of group arrival (TOGA) at multiple sites. *Journal of Atmospheric and Solar-Terrestrial Physics*, *64*(7), 817–830. https://doi.org/10.1016/S1364-6826(02)00085-8

Dwyer, J. R., & Uman, M. A. (2014). The physics of lightning. *Physics Reports*, *534*(4), 147–241. https://doi.org/10.1016/j.physrep.2013.09.004

Ferguson, J. (1998). *Computer programs for assessment of long-wavelength radio communications, version 2.0: User's guide and source files*. Space And Naval Warfare Systems Center.

Garreaud, R., Vuille, M., & Clement, A. C. (2003). The climate of the Altiplano: Observed current conditions and mechanisms of past changes. *Palaeogeography, Palaeoclimatology, Palaeoecology*, *194*(1–3), 5–22. https://doi.org/10.1016/S0031-0182(03)00269-4

GEBCO Compilation Group. (2022). GEBCO_2022 grid [Dataset]. https://doi.org/10.5285/e0f0bb80-ab44-2739-e053-6c86abc0289c

Gelaro, R., McCarty, W., Suárez, M. J., Todling, R., Molod, A., Takacs, L., et al. (2017). The Modern-Era Retrospective analysis for research and applications, version 2 (MERRA-2). *Journal of Climate*, *30*(14), 5419–5454. https://doi.org/10.1175/JCLI-D-16-0758.1

Global Modeling and Assimilation Office (GMAO). (2015). MERRA-2 inst3_3d_aer_Nv: 3d, 3-Hourly, instantaneous, model-level, assimilation, aerosol mixing ratio V5.12.4 [Dataset]. Goddard Earth Sciences Data and Information Services Center (GES DISC). https://doi.org/10.5067/LTVB4GPCOTK2

Griffiths, D. J. (2018). *Introduction to electrodynamics* (4th ed.). Cambridge University Press.

Han, Y., Luo, H., Wu, Y., Zhang, Y., & Dong, W. (2021). Cloud ice fraction governs lightning rate at a global scale. *Communications Earth & Environment*, *2*(1), 1–9. https://doi.org/10.1038/s43247-021-00233-4

Harris, G., Jr., Bowman, K. P., & Shin, D. B. (2000). Comparison of NCEP reanalysis and TRMM precipitation radar estimates of melting-layer altitudes. *Journal of Climate*, *13*(23), 4137–4148. https://doi.org/10.1175/1520-0442(2000)013<4137:coflaf>2.0.co;2

Hirsh, M. N. & Oskam, H. J. (Eds.) (1978). *Gaseous electronics*. Academic Press.

Holzworth, R. H., McCarthy, M. P., Brundell, J. B., Jacobson, A. R., & Rodger, C. J. (2019). Global distribution of superbolts. *Journal of Geophysical Research: Atmospheres*, *124*(17–18), 9996–10005. https://doi.org/10.1029/2019jd030975

Hutchins, M. L., Holzworth, R. H., Brundell, J. B., & Rodger, C. J. (2012). Relative detection efficiency of the world wide lightning location network. *Radio Science*, *47*(6), 1–9. https://doi.org/10.1029/2012RS005049

Hutchins, M. L., Holzworth, R. H., Rodger, C. J., & Brundell, J. B. (2012). Far-field power of lightning strokes as measured by the world wide lightning location network. *Journal of Atmospheric and Oceanic Technology*, *29*(8), 1102–1110. https://doi.org/10.1175/JTECH-D-11-00174.1

Ivushkin, K., Bartholomeus, H., Bregt, A. K., Pulatov, A., Kempen, B., & de Sousa, L. (2019). Global mapping of soil salinity change. *Remote Sensing of Environment*, *231*, 111260. https://doi.org/10.1016/j.rse.2019.111260

Jacobson, A. R., Holzworth, R., Harlin, J., Dowden, R., & Lay, E. (2006). Performance assessment of the world wide lightning location network (WWLLN), using the Los Alamos Sferic Array (LASA) as ground truth. *Journal of Atmospheric and Oceanic Technology*, *23*(8), 1082–1092. https://doi.org/10.1175/JTECH1902.1

Kamra, A. K. (1979). Contributions of cloud and precipitation particles to the electrical conductivity and the relaxation time of the air in thunderstorms. *Journal of Geophysical Research*, *84*(C8), 5034. https://doi.org/10.1029/JC084iC08p05034

Kanamitsu, M., Ebisuzaki, W., Woollen, J., Yang, S.-K., Hnilo, J. J., Fiorino, M., & Potter, G. L. (2002). NCEP–DOE AMIP-II reanalysis (R-2). *Bulletin of the American Meteorological Society*, *83*(11), 1631–1644. https://doi.org/10.1175/BAMS-83-11-1631

Kang, H., Jayaratne, R., & Williams, E. (2023). A new model for charge separation by proton transfer during collision between ice particles in thunderstorms. *Journal of Geophysical Research: Atmospheres*, *128*(12), e2023JD038626. https://doi.org/10.1029/2023JD038626

Kirkland, M. W. (1999). *An examination of superbolt-class lightning events observed by the FORTE satellite*. Los Alamos National Laboratory, Atmospheric Sciences Group.

Lay, E. H., Holzworth, R. H., Rodger, C. J., Thomas, J. N., Pinto, O., Jr., & Dowden, R. L. (2004). WWLL global lightning detection system: Regional validation study in Brazil. *Geophysical Research Letters*, *31*(3), L03102. https://doi.org/10.1029/2003GL018882

Lay, E. H., Jacobson, A. R., Holzworth, R. H., Rodger, C. J., & Dowden, R. L. (2007). Local time variation in land/ocean lightning flash density as measured by the World Wide Lightning Location Network. *Journal of Geophysical Research*, *112*(D13), D13111. https://doi.org/10.1029/2006JD007944

Lhermitte, R., & Williams, E. (1984). Doppler radar and electrical activity observations of a mountain thunderstorm. In *Conference on radar meteorology, ^{22}Nd* (pp. 83–90).

Li, D., Liu, F., Pérez-Invernón, F. J., Lu, G., Qin, Z., Zhu, B., & Luque, A. (2020). On the accuracy of ray-theory methods to determine the altitudes of intracloud electric discharges and ionospheric reflections: Application to narrow bipolar events. *Journal of Geophysical Research: Atmospheres*, *125*(9), e2019JD032099. https://doi.org/10.1029/2019JD032099

Magono, C. (1980). *Thunderstorms*. Elsevier.

Mazur, V., Shao, X.-M., & Krehbiel, P. R. (1998). Spider" lightning in intracloud and positive cloud-to-ground flashes. *Journal of Geophysical Research*, *103*(D16), 19811–19822. https://doi.org/10.1029/98JD02003

National Centers for Environmental Prediction, National Weather Service, NOAA, & U.S. Department of Commerce. (2000). NCEP FNL operational model global tropospheric analyses [Dataset]. Research Data Archive at the National Center for Atmospheric Research, Computational and Information Systems Laboratory. https://doi.org/10.5065/D6M043C6

Orville, R. E., Weisman, R. A., Pyle, R. B., Henderson, R. W., & Orville, R. E. (1987). Cloud-to-ground lightning flash characteristics from June 1984 through May 1985. *Journal of Geophysical Research*, *92*(D5), 5640. https://doi.org/10.1029/JD092iD05p05640

Pan, Z., Mao, F., Rosenfeld, D., Zhu, Y., Zang, L., Lu, X., et al. (2022). Coarse sea spray inhibits lightning. *Nature Communications*, *13*(1), 4289. https://doi.org/10.1038/s41467-022-31714-5

Pereyra, R. G., Bürgesser, R. E., & Ávila, E. E. (2008). Charge separation in thunderstorm conditions. *Journal of Geophysical Research*, *113*(D17), D17203. https://doi.org/10.1029/2007JD009720

Pierce, E. T. (1977). Atmospherics and radio noise. In *Lightning: Volume 1* (Vol. 1, pp. 351–384).

Pizzuti, A., Bennett, A., Soula, S., Amor, S. N., Mlynarczyk, J., Füllekrug, M., & Pédeboy, S. (2022). On the relationship between lightning superbolts and TLEs in Northern Europe. *Atmospheric Research*, *270*, 106047. https://doi.org/10.1016/j.atmosres.2022.106047

Reynolds, S. E., Brook, M., & Gourley, M. F. (1957). Thunderstorm charge separation. *Journal of the Atmospheric Sciences*, *14*(5), 426–436. https://doi.org/10.1175/1520-0469(1957)014<0426:tcs>2.0.co;2

Rodger, C. J., Brundell, J., Holzworth, R., & Lay, E. (2009). Growing detection efficiency of the world wide lightning location network. In *AIP Conference Proceedings* (Vol. 1118, No. (1), pp. 15–20). American Institute of Physics.

Rodger, C. J., Brundell, J. B., Dowden, R. L., & Thomson, N. R. (2004). Location accuracy of long distance VLF lightning location network. *Annales Geophysicae*, *22*(3), 747–758. https://doi.org/10.5194/angeo-22-747-2004

Rodger, C. J., Werner, S., Brundell, J. B., Lay, E. H., Thomson, N. R., Holzworth, R. H., & Dowden, R. L. (2006). Detection efficiency of the VLF world-Wide Lightning Location Network (WWLLN): Initial case study. *Annales Geophysicae*, *24*(12), 3197–3214. https://doi.org/10.5194/angeo-24-3197-2006

Schauwecker, S., Rohrer, M., Huggel, C., Endries, J., Montoya, N., Neukom, R., et al. (2017). The freezing level in the tropical Andes, Peru: An indicator for present and future glacier extents: The Freezing Level in the Tropical Andes. *Journal of Geophysical Research: Atmospheres*, *122*(10), 5172–5189. https://doi.org/10.1002/2016JD025943

Takahashi, T. (1978). Riming electrification as a charge generation mechanism in thunderstorms. *Journal of the Atmospheric Sciences*, *35*(8), 1536–1548. https://doi.org/10.1175/1520-0469(1978)035<1536:reaacg>2.0.co;2

Thomson, N. R. (2010). Daytime tropical D region parameters from short path VLF phase and amplitude: Daytime tropical D region parameters. *Journal of Geophysical Research*, *115*(A9), A09313. https://doi.org/10.1029/2010JA015355

Turman, B. N. (1977). Detection of lightning superbolts. *Journal of Geophysical Research*, *82*(18), 2566–2568. https://doi.org/10.1029/JC082i018p02566

Williams, E. R., Mushtak, V., Rosenfeld, D., Goodman, S., & Boccippio, D. (2005). Thermodynamic conditions favorable to superlative thunderstorm updraft, mixed phase microphysics and lightning flash rate. *Atmospheric Research*, *76*(1–4), 288–306. https://doi.org/10.1016/j.atmosres.2004.11.009

Williams, E. R. (1985). Large-scale charge separation in thunderclouds. *Journal of Geophysical Research*, *90*(D4), 6013. https://doi.org/10.1029/JD090iD04p06013

Williams, E. R. (1988). The electrification of thunderstorms. *Scientific American*, *259*(5), 88–99. https://doi.org/10.1038/scientificamerican1188-88

Williams, E. R. (2001). The electrification of severe storms. In C. A. Doswell (Ed.), *Severe convective storms* (pp. 527–561). American Meteorological Society. https://doi.org/10.1007/978-1-935704-06-5_13

Williams, E. R., Zhang, R., & Rydock, J. (1991). Mixed-phase microphysics and cloud electrification. *Journal of the Atmospheric Sciences*, *48*(19), 2195–2203. https://doi.org/10.1175/1520-0469(1991)048<2195:mpmace>2.0.co;2

WWLLN. (2022). World-Wide Lightning Location Network [Dataset]. Retrieved from http://wwlln.net/

Yair, Y., Price, C., Namia-Cohen, Y., Lynn, B., Shpund, J., & Yaffe, M. (2021). *Why are lightning super-bolts more frequent in East Mediterranean winter thunderstorms?* pico. https://doi.org/10.5194/egusphere-egu21-1474

References From the Supporting Information

Levitus, S., Locarnini, R. A., Boyer, T. P., Mishonov, A. V., Antonov, J. I., Garcia, H. E., et al. (2010). World Ocean Atlas 2009 (NOAA:1259). Retrieved from https://repository.library.noaa.gov/view/noaa/1259